

Article

# Halogenated Diazabutadiene Dyes: Synthesis, Structures, Supramolecular Features, and Theoretical Studies

Valentine G. Nenajdenko <sup>1,\*</sup> , Namiq G. Shikhaliyev <sup>2</sup>, Abel M. Maharramov <sup>2</sup>,  
Khanim N. Bagirova <sup>2</sup>, Gulnar T. Suleymanova <sup>2</sup>, Alexander S. Novikov <sup>3</sup> ,  
Victor N. Khrustalev <sup>4,5</sup>  and Alexander G. Tskhovrebov <sup>4,6,\*</sup>

<sup>1</sup> M. V. Lomonosov Moscow State University, 1, Leninskie Gory, 119991 Moscow, Russia

<sup>2</sup> Department of Organic Chemistry, Baku State University, Z. Khalilov 23, Baku 1148, Azerbaijan; namiqst@gmail.com (N.G.S.); amaharramov@bsu.edu.az (A.M.M.); stella\_stand@icloud.com (K.N.B.); gumusqiz91.sg@gmail.com (G.T.S.)

<sup>3</sup> Saint Petersburg State University, Universitetskaya Nab. 7/9, 199034 Saint Petersburg, Russia; a.s.novikov@spbu.ru

<sup>4</sup> Peoples' Friendship University of Russia, 6 Miklukho-Maklaya, 117198 Moscow, Russia; vnkhrustalev@gmail.com

<sup>5</sup> N.D. Zelinsky Institute of Organic Chemistry, Russian Academy of Sciences, 47 Leninsky Av., 119334 Moscow, Russia

<sup>6</sup> N.N. Semenov Federal Research Center for Chemical Physics, Russian Academy of Sciences, Kosygina 4, 119991 Moscow, Russia

\* Correspondence: nenajdenko@org.chem.msu.ru (V.G.N.); alexander.tskhovrebov@chph.ras.ru (A.G.T.)

Academic Editors: Ilya G. Shenderovich and Antonio Caballero

Received: 6 October 2020; Accepted: 26 October 2020; Published: 29 October 2020



**Abstract:** Novel halogenated aromatic dichlorodiazadienes were prepared via copper-mediated oxidative coupling between the corresponding hydrazones and  $\text{CCl}_4$ . These rare azo-dyes were characterized using  $^1\text{H}$  and  $^{13}\text{C}$  NMR techniques and X-ray diffraction analysis for five halogenated dichlorodiazadienes. Multiple non-covalent halogen...halogen interactions were detected in the solid state and studied by DFT calculations and topological analysis of the electron density distribution within the framework of Bader's theory (QTAIM method). Theoretical studies demonstrated that non-covalent halogen...halogen interactions play crucial role in self-assembly of highly polarizable dichlorodiazadienes. Thus, halogen bonding can dictate a packing preference in the solid state for this class of dichloro-substituted heterodienes, which could be a convenient tool for a fine tuning of the properties of this novel class of dyes.

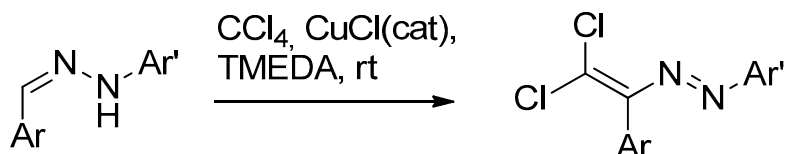
**Keywords:** non-covalent interactions; crystal engineering; halogen bonding; azo dyes; DFT; QTAIM

## 1. Introduction

Halogen bonding (XB) is one of the most intensively investigated areas in modern chemistry [1]. The field currently experiences a renaissance due to exploitation of such weak interactions for a number of functional applications, such as catalysis, drug design, nonlinear optics, reactivity control, and construction of functional supramolecular architectures [2–10]. Utilization of non-covalent interactions lies at the foundation of the design supramolecular materials and control of their ultimate architectures [11–14]. XB has recently emerged as a powerful tool for the creation of such materials due to its stability, directionality and reversibility [15–17]. In this context, halogen-halogen interactions received particular attention and were intensively explored both experimentally and

theoretically [18–21]. Arguably, XB can be more beneficial than the hydrogen bonding in the construction of functional materials and tuning their properties due to its higher directionality [10,22,23].

Recently, we discovered a novel class of azo-dyes, i.e., dichlorodiazadienes, which can be easily prepared via unprecedented copper-catalyzed reaction between  $\text{CCl}_4$  with *N*-substituted hydrazones (Scheme 1) [24]. Currently, very little is known about the chemistry and properties of these dichloro-substituted heterodienes [25–31].

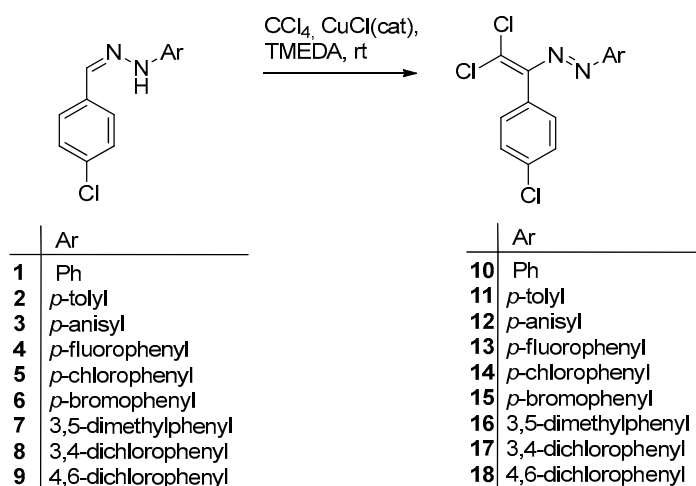


**Scheme 1.** Copper-catalyzed synthesis of dichlorodiazadienes.

Following our interest in construction of supramolecular architectures via non-covalent interactions [32–39] and chemistry of novel diazadienes, we report now the synthesis of halogenated dichlorodiazadienes to demonstrate that dichloro-substituted heterodiene fragment can behave as a strong XB donor/acceptor, what can be used in the design of heterodiene azo-dyes and their self-assembly in the solid state. Incorporation of a halogen atom(s) in the dichloro-dyes' backbone completely changes the way the colorants self-assemble in the crystal. Thus, we show that the XB can dictate a packing preference in the solid state for this class of dichloro-substituted heterodienes. In addition, we performed DFT calculations and topological analysis of the electron density distribution within the formalism of Bader's theory (QTAIM method), which support the presence of intermolecular non-covalent interactions halogen...halogen (Hal...Hal) in the solid state.

## 2. Results and Discussion

The target halogenated azabutadienes **10–18** were synthesized by  $\text{Cu}^{\text{I}}$ -catalyzed reaction between the corresponding hydrazones **1–9** and  $\text{CCl}_4$  and isolated in up to 82% yield as red crystalline solids (Scheme 2).



**Scheme 2.** Copper-catalyzed synthesis of dichlorodiazadienes.

The structure of **10–18** was confirmed by the  $^1\text{H}$  and  $^{13}\text{C}$  NMR spectroscopies and X-ray diffraction analysis for **10**, **13–15**, and **17** (Figures 1–4).  $^1\text{H}$  NMR and  $^{13}\text{C}\{^1\text{H}\}$  spectra ( $\text{CDCl}_3$ ) are consistent with their solid-state structures. Dyes **10**, **13–15**, and **17** could be easily recrystallized to produce large red crystals, suitable for analysis by single crystal X-ray crystallography. The structural investigations confirmed the formation of azabutadienes. Overall, metrical parameters for **10**, **13–15**, and **17** are

similar to those reported for similar azabutadienes [26,29–31]. However, introduction of halogen atoms in the dichloro-dyes' backbone has a dramatic impact on its self-assembly in the crystal. In the crystal packing of **10** (para-chloro substitution at the phenyl, attached the double C=C bond) dye molecules form shifted columns (Figure 1) via  $\pi$ - $\pi$  interactions. The columns dimerize in the crystal via Cl $\cdots$ Cl attractive interactions between the neighboring dye molecules (type 2 contacts) [23]. The dichloroalkene acts as a donor of the halogen bond here (Figure 1).

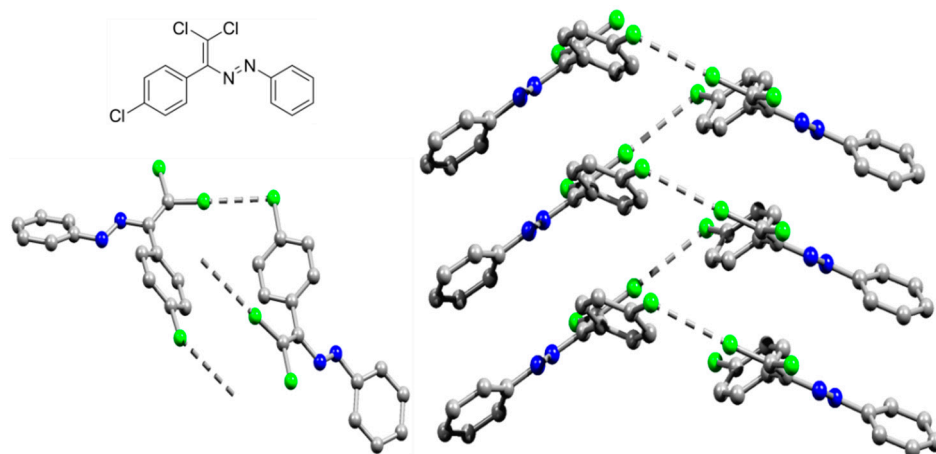


**Figure 1.** Ball-and-stick representation of **10** and its self-assembly via Cl $\cdots$ Cl bonding in the crystal. Blue, green and grey spheres represent nitrogen, chlorine, carbon atoms, respectively. Hydrogen atoms were omitted for clarity.

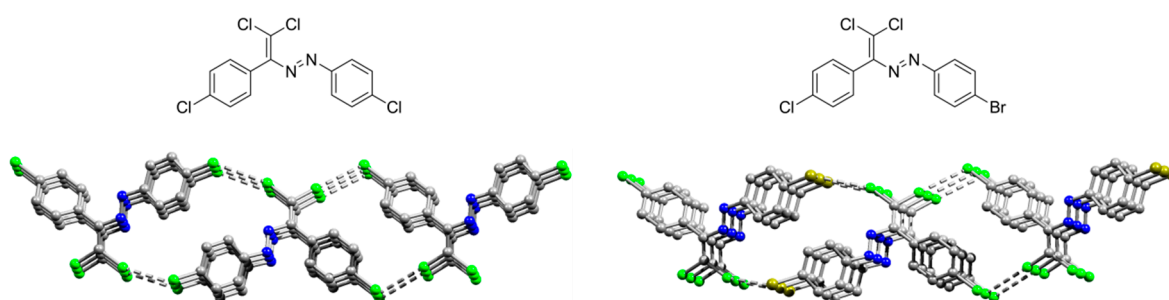


**Figure 2.** Ball-and-stick representations of **14** and **15** and their self-assembly via Cl $\cdots$ Hal bonding in the crystal. Olive-green, blue, green, and grey spheres represent bromine, nitrogen, chlorine, and carbon atoms, respectively. Hydrogen atoms were omitted for clarity.

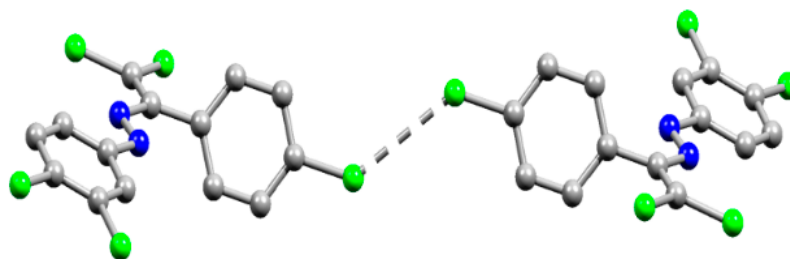


**Figure 3.** Ball-and-stick representation of **17** and its supramolecular dimerization via Cl $\cdots$ Cl type 1 bonding in the crystal. Blue, green, and grey spheres represent nitrogen, chlorine, and carbon atoms, respectively. Hydrogen atoms were omitted for clarity.

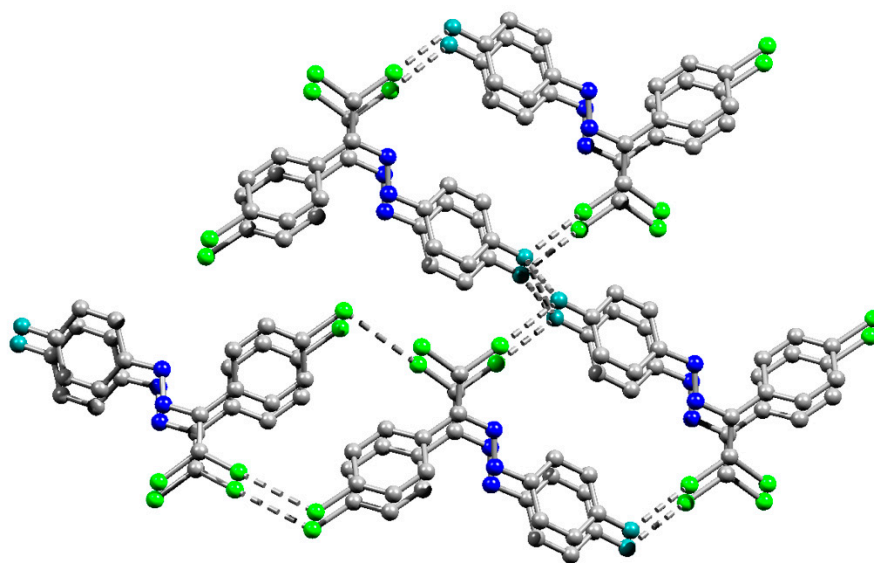


**Figure 4.** Ball-and-stick representation of **13** and its self-assembly via Cl...Cl bonding in the crystal. Blue, green, and grey and cyan spheres represent nitrogen, chlorine, carbon, and fluorine atoms, respectively. Hydrogen atoms were omitted for clarity.

Functionalization of dichloro-dyes with another extra halogen atom (compounds **14** and **15**) does not prevent the formation of columns and supramolecular dimerization via Cl...Cl interactions in the crystal (Figure 2). In addition to this, the columns in the crystal of **14** and **15** interact with another neighboring columns via Cl...Hal (Hal=Cl(**14**), Br(**15**)) type 2 bonding forming 3D supramolecular frameworks (Figure 2).

Introduction of one more halogen atom in the dichloro-dyes' backbone completely changes its self-assembly in the crystal. Remarkably, crystal packing of **17** features only one type of Hal...Hal interaction between the chlorines of the *p*-chlorophenyl groups (Figure 3), which refer to repulsive type 1 contacts. Halogen atoms, attached to the alkene or dichlorobenzene moieties do not form any halogen bonding. Such a behavior is not very clear at the moment and requires additional studies. One plausible explanation is insufficient nucleophilicity of halogens in **17** for the formation of type 2 contacts.

Finally, when dichloro-dyes are functionalized with the fluorine atom (**13**, *para*-substitution at the phenyl, attached the double C=C bond, Figure 4), the situation with self-assembly in the crystal is similar to the brominated or chlorinated analogs **14** and **15**. The columns form 3D supramolecular frameworks via Cl...Cl and Cl...F type 2 contacts. An interesting peculiarity of self-assembly of **13** in the crystal is the formation of Cl...F type 1 contacts (Figure 4). Thus, the crystal structure of **13** features a bifurcated XB and a remarkable combination of type 1 and 2 halogen contacts (Figure 4).

Inspection of the crystallographic data suggests the presence of multiple intermolecular non-covalent interactions Hal...Hal in the crystals of **10**, **13–15**, and **17**. Indeed, the observed distances Hal...Hal are shorter than the sum of Bondi's vdW radii for the corresponding atoms [40]. Thus, in addition to structural analysis, a detailed computational studies were desired. In order to understand the nature and quantify energies of various short halogen-halogen contacts the DFT calculations followed by the topological analysis of the electron density distribution within the QTAIM approach [41] were carried out at the  $\omega$ B97XD/6-311++G\*\* level of theory for model supramolecular associates containing all types of these noncovalent interactions (see Computational details and Table S1 in the Supplementary Materials). Results of QTAIM analysis summarized in Table 1, the contour line diagrams of the Laplacian of electron density distribution  $\nabla^2\rho(r)$ , bond paths, and selected zero-flux surfaces as well as visualization of electron localization function (ELF) analysis for selected short halogen-halogen contacts shown in Figure 5 for illustrative purposes.

**Table 1.** Values of the density of all electrons— $\rho(r)$ , Laplacian of electron density— $\nabla^2\rho(r)$  and appropriate  $\lambda_2$  eigenvalues (with promolecular approximation), energy density— $H_b$ , potential energy density— $V(r)$ , and Lagrangian kinetic energy— $G(r)$  (a.u.) at the bond critical points (3, -1), corresponding to various short halogen-halogen contacts in **10**, **13–15**, and **17**, and estimated energies for these interactions  $E_{\text{int}}$  (kcal/mol).

Halogen–Halogen Contact	$\rho(r)$	$\nabla^2\rho(r)$	$\lambda_2$	$H_b$	$V(r)$	$G(r)$	$E_{\text{int}}^a$	$E_{\text{int}}^b$
<b>10</b> Cl...Cl, 3.377 Å (96% from the sum of Bondi's vdW radii)	0.008	0.031	−0.012	0.002	−0.004	0.006	1.2	1.8
<b>13</b> F...F, 2.864 Å (97% from the sum of Bondi's vdW radii)	0.006	0.031	−0.007	0.001	−0.006	0.007	≈2*	≈2*
<b>13</b> F...F, 2.917 Å (99% from the sum of Bondi's vdW radii)	0.007	0.031	−0.008	0.001	−0.006	0.007	≈2*	≈2*
<b>13</b> Cl...F, 2.963 Å (92% from the sum of Bondi's vdW radii)	0.009	0.042	−0.013	0.001	−0.008	0.009	2.5	2.7
<b>13</b> Cl...Cl, 3.405 Å (97% from the sum of Bondi's vdW radii)	0.007	0.029	−0.011	0.002	−0.004	0.006	1.2	1.8
<b>14</b> Cl...Cl, 3.463 Å (99% from the sum of Bondi's vdW radii)	0.007	0.026	−0.009	0.002	−0.003	0.005	0.9	1.5
<b>14</b> Cl...Cl, 3.399 Å (97% from the sum of Bondi's vdW radii)	0.007	0.029	−0.011	0.002	−0.004	0.006	1.2	1.8
<b>15</b> Cl...Br, 3.637 Å (102% from the sum of Bondi's vdW radii)	0.006	0.021	−0.008	0.001	−0.003	0.004	0.9	1.2
<b>15</b> Cl...Cl, 3.394 Å (97% from the sum of Bondi's vdW radii)	0.007	0.030	−0.011	0.002	−0.004	0.006	1.2	1.8
<b>17</b> Cl...Cl, 3.469 Å (99% from the sum of Bondi's vdW radii)	0.007	0.027	−0.009	0.002	−0.004	0.005	1.2	1.5

<sup>a</sup>  $E_{\text{int}} = 0.49(-V(r))$  (this correlation between the interaction energy and the potential energy density of electrons at the bond critical points (3, -1) was specifically developed for noncovalent interactions involving chlorine atoms) [42]. <sup>b</sup>  $E_{\text{int}} = 0.47G(r)$  (this correlation between the interaction energy and the kinetic energy density of electrons at the bond critical points (3, -1) was specifically developed for noncovalent interactions involving chlorine atoms) [42]. \* There are no generally accepted specific correlations between the interaction energy and the potential or kinetic energy densities of electrons at the bond critical points (3, -1) for F...F noncovalent interactions, but it is clearly expected from values of  $V(r)$  and  $G(r)$  that strength of these contacts in **13** is approx. 2 kcal/mol.

The QTAIM analysis of **10**, **13–15**, and **17** demonstrates the presence of bond critical points (3, -1) for all weak contacts presented in Table 1. The low magnitude of the electron density (0.006–0.009 a.u.), positive values of the Laplacian of electron density (0.021–0.042 a.u.), and very close to zero positive energy density (0.001–0.002 a.u.) in these bond critical points (3, -1) are typical for halogen-halogen noncovalent interactions [5,39,43]. The balance between the potential and kinetic energy densities of electrons at the bond critical points (3, -1) for studied weak contacts in **10**, **13–15**, and **17** reveals that a covalent contribution is absent in these interactions [44] (Table 1). The Laplacian of electron density is typically decomposed into the sum of contributions along the three principal axes of maximal variation, giving the three eigenvalues of the Hessian matrix ( $\lambda_1$ ,  $\lambda_2$  and  $\lambda_3$ ), and the sign of  $\lambda_2$  can be utilized to distinguish bonding (attractive,  $\lambda_2 < 0$ ) weak interactions from non-bonding ones (repulsive,  $\lambda_2 > 0$ ) [45,46]. Thus, discussed noncovalent interactions in **10**, **13–15**, and **17** are attractive (Table 1). Overall, it follows from the results of theoretical calculations that all short halogen-halogen contacts in **10**, **13–15**, and **17** are very similar in terms of energies (their estimated strength per one contact vary from 1 to 3 kcal/mol), which correlates well with very close values of minimal and maximal electrostatic surface potentials on halogen atoms in isolated molecules **10**, **13–15**, and **17** (Figure S1 in the Supplementary Materials).

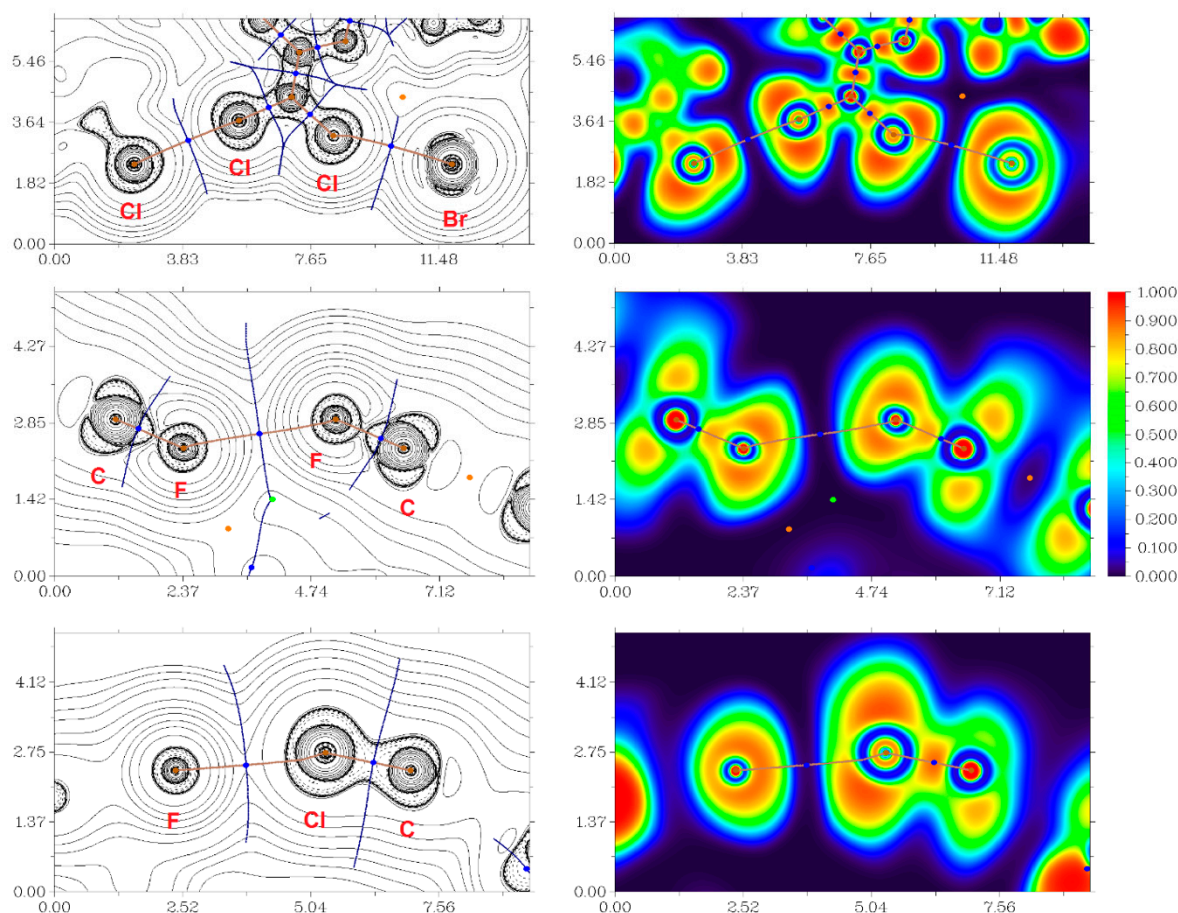


**Figure 5.** Contour line diagrams of the Laplacian of electron density distribution  $\nabla^2\rho(r)$ , bond paths, and selected zero-flux surfaces (left) and visualization of electron localization function (ELF) analysis (right) for intermolecular Cl...Br and Cl...Cl contacts in **15** (top); F...F (center) and Cl...F (bottom) contacts in **13**. Bond critical points (3, -1) are shown in blue, nuclear critical points (3, -3)—in pale brown, ring critical points (3, +1)—in orange, cage critical points (3, +3)—in light green, length units—Å, bond paths are shown as pale brown lines, and the color scale for the ELF maps is presented in a.u.

To understand what kind of interatomic contacts give the largest contributions in crystal packing, we carried out the Hirshfeld surface analysis for all obtained X-ray structures **10**, **13–15**, and **17** (Table 2 and Figure 6). The Hirshfeld surface analysis for the X-ray structures **10**, **13–15**, and **17** reveals that in all cases crystal packing determined primarily by interatomic contacts involving chlorine and hydrogen atoms.

**Table 2.** Main partial contributions of different interatomic contacts to the Hirshfeld surfaces of X-ray structures **10**, **13–15**, and **17**.

X-Ray Structure	Contributions of Different Interatomic Contacts to the Hirshfeld Surfaces
<b>10</b>	Cl-H 37.4%, H-H 21.0%, C-H 15.8%, C-C 7.9%, Cl-Cl 5.9%, N-H 5.8%, N-C 3.0%, -Cl-C 2.9%, Cl-N 0.1%
<b>13</b>	Cl-H 32.6%, H-H 16.2%, C-H 14.6%, C-C 7.4%, Cl-Cl 6.1%, N-H 5.8%, Cl-F 4.1%, N-C 3.1%, Cl-C 3.0%, F-H 2.8%, F-F 2.5%, F-C 1.7%
<b>14</b>	Cl-H 33.5%, H-H 17.1%, Cl-Cl 15.7%, C-H 12.6%, C-C 8.5%, N-H 5.2%, Cl-C 4.1%, N-C 3.2%, N-N 0.1%
<b>15</b>	Cl-H 30.7%, H-H 15.7%, C-H 13.0%, C-C 8.1%, Cl-Cl 5.8%, Br-Cl 5.7%, N-H 5.2%, Br-H 4.6%, Br-Br 3.8%, N-C 3.2%, Cl-C 2.2%, Br-C 1.8%, N-N 0.1%
<b>17</b>	Cl-H 44.6%, Cl-C 15.6%, H-H 10.5%, Cl-Cl 8.2%, C-H 8.1%, Cl-N 5.1%, C-C 4.4%, N-C 1.9%, N-H 1.5%

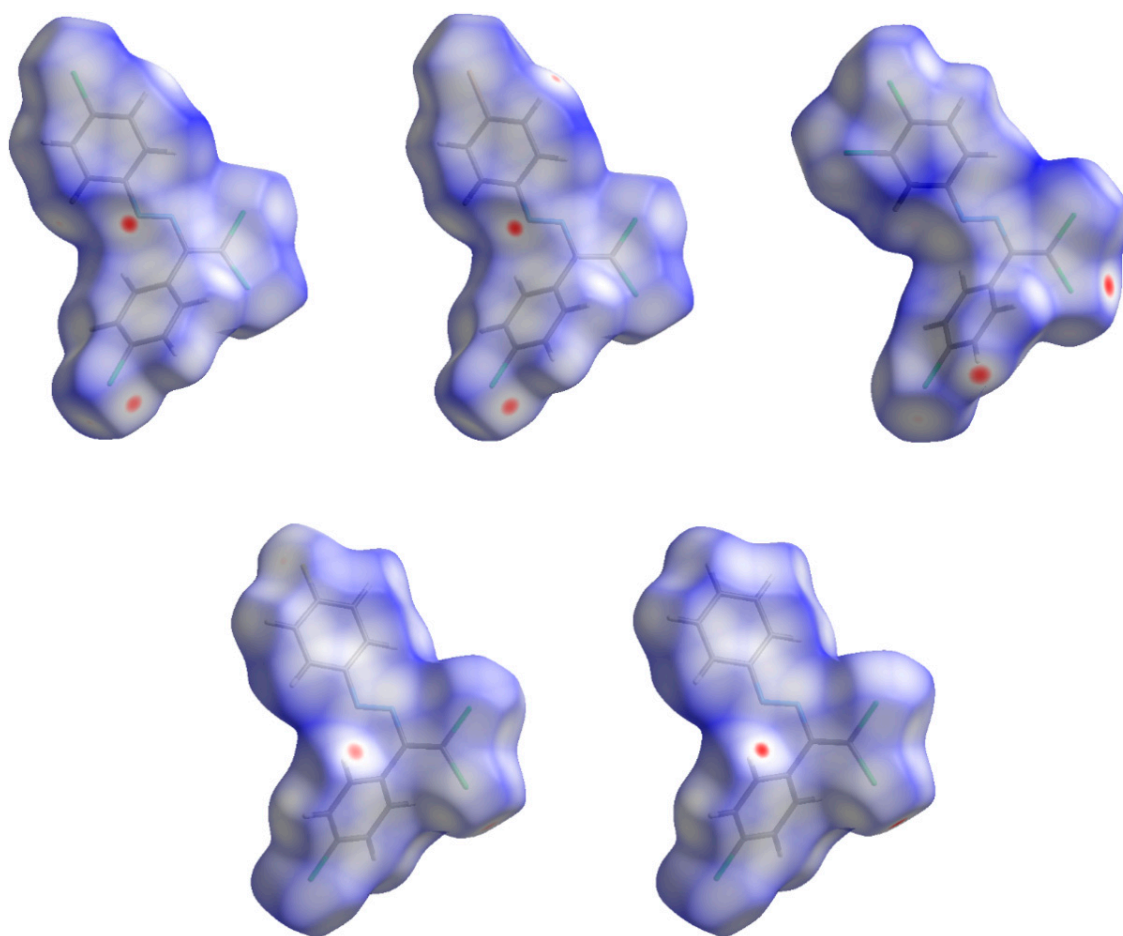


**Figure 6.** Visualization of Hirshfeld surfaces for X-ray structures **14**, **15**, and **17** (top), **13** and **10** (bottom).

### 3. Materials and Methods

**General remarks.** Unless stated otherwise, all the reagents used in this study were obtained from the commercial sources (Aldrich, TCI-Europe, Strem, ABCR). NMR spectra were recorded on a Bruker Avance 300 ( $^1\text{H}$ : 300 MHz, Karlsruhe, Germany); chemical shifts ( $\delta$ ) are given in ppm relative to TMS, coupling constants ( $J$ ) in Hz. The solvent signals were used as references ( $\text{CDCl}_3$ :  $\delta_{\text{C}} = 77.16$  ppm; residual  $\text{CHCl}_3$  in  $\text{CDCl}_3$ :  $\delta_{\text{H}} = 7.26$  ppm;  $\text{CD}_2\text{Cl}_2$ :  $\delta_{\text{C}} = 53.84$  ppm; residual  $\text{CH}_2\text{Cl}_2$  in  $\text{CD}_2\text{Cl}_2$ :  $\delta_{\text{H}} = 5.32$  ppm);  $^1\text{H}$  and  $^{13}\text{C}$  assignments were established using NOESY, HSQC, and HMBC experiments; numbering schemes as shown in the Inserts. IR: Perkin-Elmer Spectrum One spectrometer (Waltham, MA, USA.), wavenumbers ( $\tilde{\nu}$ ) in  $\text{cm}^{-1}$ . Mass-spectra were obtained on a Bruker micrOTOF spectrometer equipped with electrospray ionization (ESI) source (Bremen, Germany); MeOH,  $\text{CH}_2\text{Cl}_2$ , or MeOH/ $\text{CH}_2\text{Cl}_2$  mixture was used as a solvent. Thermogravimetric analysis (TGA) and differential thermal analysis were determined using a Netzsch TG 209F1 Libra apparatus (Selb, Germany). Solvents were purified by distillation over the indicated drying agents and were transferred under Ar:  $\text{Et}_2\text{O}$  (Mg/anthracene),  $\text{CH}_2\text{Cl}_2$  ( $\text{CaH}_2$ ), hexane (Na/K). Flash chromatography: Merck Geduran<sup>®</sup> Si 60 (Darmstadt, Germany) (40–63  $\mu\text{m}$ ).

The single point calculations based on the experimental X-ray geometries of **10**, **13–15**, and **17** have been carried out at the DFT level of theory using the dispersion-corrected hybrid functional  $\omega\text{B97XD}$  [47] with the help of Gaussian-09 program package ([M. J. Frisch et al., Gaussian-09, Revision C.01, Gaussian, Inc., Wallingford CT, USA, 2010.], full citation for this program is given in the SI). The 6-311++G\*\* basis sets [48–51] were used for all atoms. The topological analysis of the electron density distribution with the help of the atoms in molecules (QTAIM) method developed by Bader [41] has been performed by using the Multiwfn program (version 3.6, Beijing, China) [52]. The Cartesian atomic coordinates for

model supramolecular associates are presented in Table S1, Supporting Information. The Hirshfeld surfaces analysis has been performed by using the CrystalExplorer program (version 17.5, Perth, Australia) [53]. The normalized contact distances ( $d_{\text{norm}}$ ) [54] based on Bondi's van der Waals radii [40] were mapped into the Hirshfeld surfaces.

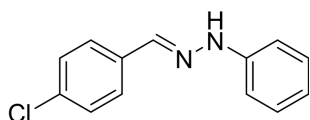
### 3.1. Crystal Structure Determination

X-ray diffraction data for **10**, **13–15**, and **17** were collected at the 'RSA' beamline ( $\lambda = 0.80246 \text{ \AA}$ ) of the Kurchatov Synchrotron Radiation Source. All datasets were collected at 100 K. In total, 720 frames were collected with an oscillation range of 1.0 in the  $\varphi$  scanning mode using two different orientations for each crystal. The semi-empirical correction for absorption was applied using the Scala program [55]. The data were indexed and integrated using the utility iMOSFLM from the CCP4 software suite [56,57]. For details, see Table S1. The structures were solved by intrinsic phasing modification of direct methods [58] and refined by a full-matrix least-squares technique on  $F^2$  with anisotropic displacement parameters for all non-hydrogen atoms. The hydrogen atoms were placed in calculated positions and refined within the riding model with fixed isotropic displacement parameters [ $U_{\text{iso}}(\text{H}) = 1.5U_{\text{eq}}(\text{C})$  for the methyl groups and  $1.2U_{\text{eq}}(\text{C})$  for the other groups]. All calculations were carried out using the SHELXTL program [59,60].

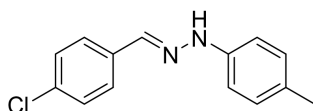
Crystallographic data for **10**, **13–15**, and **17** have been deposited with the Cambridge Crystallographic Data Center, CCDC 2035010-2035014, respectively. Copies of this information may be obtained free of charge from the Director, CCDC, 12 Union Road, Cambridge CB2 1EZ, UK (fax: +44-1223-336033; e-mail: edeposit@ccdc.cam.ac.uk or [www.ccdc.cam.ac.uk](http://www.ccdc.cam.ac.uk)).

### 3.2. Synthetic Part

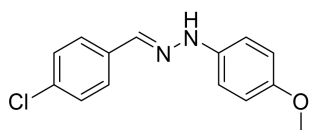
Schiff bases **1–9** were synthesized according to the reported method [20,21]. A mixture of (2-nitrophenyl)hydrazine (10.2 mmol),  $\text{CH}_3\text{COONa}$  (0.82 g) and a corresponding 4-substituted aldehyde (10 mmol) were refluxed with stirring in ethanol (50 mL) for 2 h. The reaction mixture was cooled to room temperature and water (50 mL) was added to give a precipitate of crude product, which was filtered off, washed with diluted ethanol (1:1 with water) and dried in vacuo.



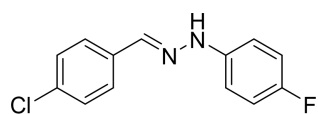
**1.** White solid (69%), mp 118 °C.  $^1\text{H NMR}$  (300 MHz,  $\text{DMSO-}d_6$ )  $\delta$  10.46 (s, 1H, NH), 7.85 (s, 1H, CH), 7.66 (d,  $J = 8.4 \text{ Hz}$ , 2H, arom), 7.43 (d,  $J = 8.4 \text{ Hz}$ , 2H, arom), 7.23 (t,  $J = 7.7 \text{ Hz}$ , 2H, arom), 7.09 (d,  $J = 7.9 \text{ Hz}$ , 2H, arom), 6.76 (t,  $J = 7.2 \text{ Hz}$ , 1H, arom).  $^{13}\text{C NMR}$  (75 MHz,  $\text{DMSO-}d_6$ )  $\delta$  145.5, 135.4, 135.2, 132.5, 129.5, 129.1, 127.5, 119.41, 112.5.



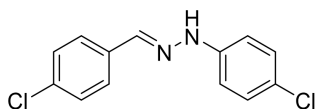
**2.** White solid (92%), mp 151 °C.  $^1\text{H NMR}$  (300 MHz,  $\text{DMSO-}d_6$ )  $\delta$  10.33 (s, 1H, NH), 7.80 (s, 1H, CH), 7.66 (s, 1H, arom), 7.42 (d,  $J = 8.4 \text{ Hz}$ , 2H, arom), 7.00 (q,  $J = 8.4 \text{ Hz}$ , 5H, arom), 2.09 (s, 3H,  $\text{CH}_3$ ).  $^{13}\text{C NMR}$  (75 MHz,  $\text{DMSO-}d_6$ )  $\delta$  138.6, 130.8, 130.1, 127.7, 125.4, 124.5, 123.3, 122.8, 107.92, 16.1.



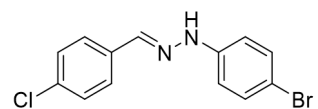
**3.** White solid (87%), mp 141 °C.  $^1\text{H NMR}$  (300 MHz,  $\text{DMSO-}d_6$ )  $\delta$  10.24 (s, 1H, NH), 7.78 (s, 1H, CH), 7.63 (d,  $J = 8.5 \text{ Hz}$ , 2H, arom), 7.41 (d,  $J = 8.5 \text{ Hz}$ , 2H, arom), 7.01 (d,  $J = 8.9 \text{ Hz}$ , 2H, arom), 6.84 (d,  $J = 8.9 \text{ Hz}$ , 2H, arom), 3.69 (s, 3H,  $\text{OCH}_3$ ).  $^{13}\text{C NMR}$  (75 MHz,  $\text{DMSO-}d_6$ )  $\delta$  153.2, 139.5, 135.5, 134.2, 132.1, 129.0, 127.3, 115.0, 113.5, 55.7.



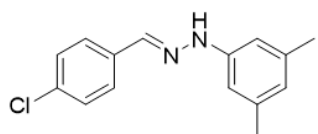
4. White solid (77%), mp 135 °C.  $^1\text{H}$  NMR (300 MHz,  $\text{DMSO-}d_6$ )  $\delta$  7.02 (d, 2H,  $J = 6.0$  Hz), 7.22 (t, 2H,  $J = 9.1$  Hz), 7.37 (d, 2H,  $J = 9.1$  Hz), 7.68–7.73(m, 2H), 7.87(s, 1H), 10.49 (s, 1H).  $^{13}\text{C}$  NMR (75 MHz,  $\text{DMSO-}d_6$ )  $\delta$  114.3, 115.9, 116.2, 128.0, 132.1, 132.63, 136.7, 145.0, 109.9.



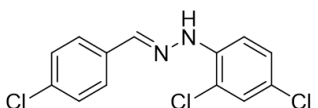
5. White solid (76%), mp 153 °C.  $^1\text{H}$  NMR (300 MHz,  $\text{DMSO-}d_6$ )  $\delta$  10.58 (s, 1H, NH), 7.85 (s, 1H, CH), 7.67 (d,  $J = 8.3$  Hz, 2H, arom), 7.48–7.38 (m, 2H, arom), 7.25 (d,  $J = 8.7$  Hz, 2H, arom), 7.07 (d,  $J = 8.7$  Hz, 2H, arom).  $^{13}\text{C}$  NMR (75 MHz,  $\text{DMSO-}d_6$ )  $\delta$  144.4, 136.3, 135.0, 132.8, 129.3, 129.1, 127.7, 122.6, 113.9.



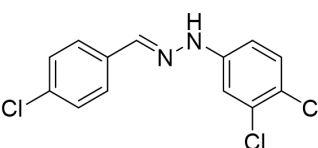
6. White solid (94%), mp 131 °C.  $^1\text{H}$  NMR (300 MHz,  $\text{DMSO-}d_6$ )  $\delta$  10.59 (s, 1H, NH), 7.85 (s, 1H, CH), 7.67 (d,  $J = 8.5$  Hz, 2H, arom), 7.43 (d,  $J = 8.5$  Hz, 2H, arom), 7.37 (d,  $J = 8.8$  Hz, 2H, arom), 7.03 (d,  $J = 8.8$  Hz, 2H, arom).  $^{13}\text{C}$  NMR (75 MHz,  $\text{DMSO-}d_6$ )  $\delta$  144.8, 136.4, 134.9, 132.8, 132.2, 129.1, 127.7, 114.4, 110.2, 39.9.



7. White solid (72%), mp 119 °C.  $^1\text{H}$  NMR (300 MHz,  $\text{DMSO-}d_6$ )  $\delta$  10.30 (s, 1H, NH), 7.81 (s, 1H, CH), 7.65 (d,  $J = 8.5$  Hz, 2H, arom), 7.42 (d,  $J = 8.5$  Hz, 2H, arom), 6.69 (s, 2H, arom), 6.41 (s, 1H, arom), 2.22 (s, 6H,  $\text{CH}_3$ ).  $^{13}\text{C}$  NMR (75 MHz,  $\text{DMSO-}d_6$ )  $\delta$  145.3, 138.5, 135.3, 135.0, 132.3, 129.1, 127.5, 121.3, 110.3, 21.7.



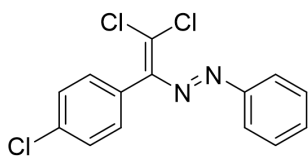
8. White solid (88%), mp 114 °C.  $^1\text{H}$  NMR (300 MHz,  $\text{DMSO-}d_6$ )  $\delta$  10.16 (s, 1H, NH), 8.28 (s, 1H, CH), 7.69 (d,  $J = 8.7$  Hz, 2H, arom), 7.56 (d,  $J = 8.7$  Hz, 1H, arom), 7.51–7.43 (m, 3H, arom), 7.35–7.17 (m, 1H, arom).  $^{13}\text{C}$  NMR (75 MHz,  $\text{DMSO-}d_6$ )  $\delta$  162.3, 140.9, 140.1, 134.6, 133.4, 129.2, 129.0, 128.5, 128.1, 122.8, 117.1, 115.5.



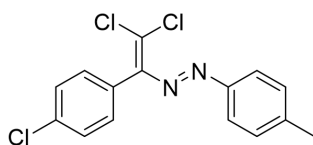
9. White solid (92%), mp 112 °C.  $^1\text{H}$  NMR (300 MHz,  $\text{DMSO-}d_6$ )  $\delta$  10.74 (s, 1H, NH), 7.90 (d,  $J = 14.3$  Hz, 1H), 7.69 (d,  $J = 8.3$  Hz, 2H, arom), 7.44 (q,  $J = 8.3, 7.5$  Hz, 3H, arom), 7.26 (s, 1H, CH), 7.00 (d,  $J = 8.4$  Hz, 1H, arom).  $^{13}\text{C}$  NMR (75 MHz,  $\text{DMSO-}d_6$ )  $\delta$  145.6, 137.6, 134.6, 133.2, 132.1, 131.5, 131.3, 130.2, 129.8, 129.1, 128.0, 120.1, 113.3, 112.8.

### 3.3. Synthesis of Dichlorodiazadiens

A twenty-milliliter screw neck vial was charged with DMSO (10 mL), 1–9 (1 mmol), tetramethylethylenediamine (TMEDA) (295 mg, 2.5 mmol), CuCl (2 mg, 0.02 mmol), and  $\text{CCl}_4$  (20 mmol, 10 equiv). After 3 h (until TLC analysis showed complete consumption of corresponding Schiff base) reaction mixture was poured into ~0.01 M solution of HCl (100 mL, ~pH = 2), and extracted with dichloromethane ( $3 \times 20$  mL). The combined organic phase was washed with water ( $3 \times 50$  mL), brine (30 mL), dried over anhydrous  $\text{Na}_2\text{SO}_4$  and concentrated in vacuo. The residue was purified by column chromatography on silica gel using appropriate mixtures of hexane and dichloromethane (3/1–1/1).

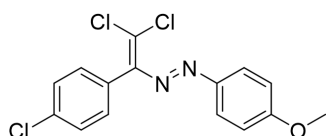


**10.** Red solid (73%), mp 85 °C.  $^1\text{H NMR}$  (300 MHz,  $\text{CDCl}_3$ )  $\delta$  7.71–7.60 (m, 2H, arom), 7.35 (dd,  $J = 7.6, 3.8$  Hz, 4H, arom), 7.28 (s, 1H, arom), 7.03 (d,  $J = 8.3$  Hz, 2H, arom).  $^{13}\text{C NMR}$  (75 MHz,  $\text{CDCl}_3$ )  $\delta$  134.6, 131.7, 131.3, 130.7, 129.4, 129.0, 128.4, 127.1, 126.2, 123.1.

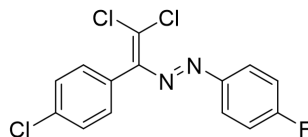


**11.** Red solid (79%), mp 90 °C.  $^1\text{H NMR}$  (300 MHz,  $\text{CDCl}_3$ )  $\delta$  7.69 (d,  $J = 8.2$  Hz, 2H, arom), 7.42 (d,  $J = 8.3$  Hz, 2H, arom), 7.26 (d,  $J = 8.2$  Hz, 2H, arom), 7.13 (d,  $J = 8.3$  Hz, 2H, arom), 2.42 (s, 3H,  $\text{CH}_3$ ).  $^{13}\text{C NMR}$  (75 MHz,  $\text{CDCl}_3$ )  $\delta$  162.3, 151.2, 150.9, 142.5, 134.7, 131.4, 131.0, 129.7, 128.4, 123.2, 21.5.

Crystals, suitable for X-ray analysis, were obtained by the slow evaporation of saturated hexane/EtOAc (5/1) solution.

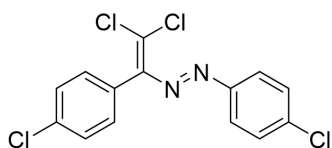


**12.** Red solid (72%), mp 96 °C.  $^1\text{H NMR}$  (300 MHz,  $\text{CDCl}_3$ )  $\delta$  7.78 (d,  $J = 9.0$  Hz, 2H, arom), 7.42 (d,  $J = 8.4$  Hz, 2H, arom), 7.13 (d,  $J = 8.4$  Hz, 2H, arom), 6.95 (d,  $J = 9.0$  Hz, 2H, arom), 3.88 (s, 3H,  $\text{OCH}_3$ ).  $^{13}\text{C NMR}$  (75 MHz,  $\text{CDCl}_3$ )  $\delta$  162.7, 162.3, 151.1, 147.2, 134.6, 131.4, 131.2, 128.4, 125.3, 114.2, 55.6.



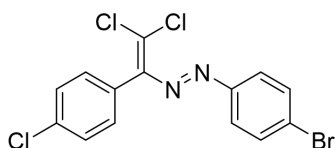
**13.** Red solid (68%), mp 77 °C.  $^1\text{H NMR}$  (300 MHz,  $\text{CDCl}_3$ )  $\delta$  7.81 (dd,  $J = 8.6, 5.4$  Hz, 2H), 7.43 (d,  $J = 8.3$  Hz, 2H), 7.14 (t,  $J = 8.8$  Hz, 4H).  $^{13}\text{C NMR}$  (75 MHz,  $\text{CDCl}_3$ )  $\delta$  167.6, 166.4, 151.1, 149.3, 134.8, 131.4, 130.8, 129.6, 128.5, 125.4, 116.2, 115.9.

Crystals, suitable for X-ray analysis, were obtained by the slow evaporation of saturated hexane/EtOAc (5/1) solution.



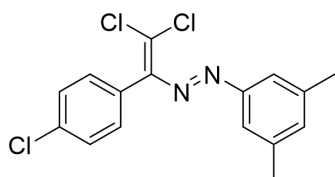
**14.** Red solid (67%), mp 94 °C.  $^1\text{H NMR}$  (300 MHz,  $\text{CDCl}_3$ )  $\delta$  7.73 (d,  $J = 8.6$  Hz, 1H), 7.43 (d,  $J = 8.4$  Hz, 2H), 7.12 (d,  $J = 8.4$  Hz, 1H).  $^{13}\text{C NMR}$  (75 MHz,  $\text{CDCl}_3$ )  $\delta$  162.3, 151.1, 137.7, 136.5, 134.9, 131.4, 130.6, 129.3, 128.5, 124.4.

Crystals, suitable for X-ray analysis, were obtained by the slow evaporation of saturated hexane/EtOAc (5/1) solution.

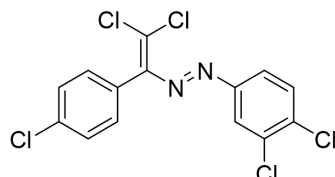


**15.** Red solid (70%), mp 105 °C.  $^1\text{H NMR}$  (300 MHz,  $\text{CDCl}_3$ )  $\delta$  7.69–7.56 (m, 4H, arom), 7.49–7.39 (m, 2H, arom), 7.12 (d,  $J = 8.4$  Hz, 2H, arom).  $^{13}\text{C NMR}$  (75 MHz,  $\text{CDCl}_3$ )  $\delta$  151.4, 134.9, 132.3, 131.4, 130.6, 129.8, 128.5, 127.4, 126.3, 124.6.

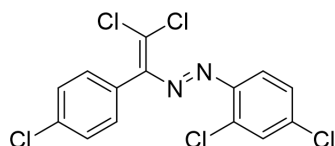
Crystals, suitable for X-ray analysis, were obtained by the slow evaporation of saturated hexane/EtOAc (5/1) solution.



**16.** Red solid (82%), mp 145 °C.  $^1\text{H}$  NMR (300 MHz,  $\text{CDCl}_3$ )  $\delta$  7.44 (d,  $J = 7.7$  Hz, 4H, arom), 7.15 (d,  $J = 7.7$  Hz, 3H, arom), 2.40 (s, 6H,  $\text{CH}_3$ ).  $^{13}\text{C}$  NMR (75 MHz,  $\text{CDCl}_3$ )  $\delta$  157.7, 148.3, 146.7, 134.2, 130.2, 129.0, 126.8, 126.5, 123.9, 116.5, 16.6.



**17.** Red solid (66%), mp 115 °C.  $^1\text{H}$  NMR (300 MHz,  $\text{CDCl}_3$ )  $\delta$  7.89 (s, 1H, arom), 7.68–7.61 (m, 1H, arom), 7.54 (d,  $J = 8.6$  Hz, 1H, arom), 7.44 (d,  $J = 8.3$  Hz, 2H, arom), 7.11 (d,  $J = 8.3$  Hz, 2H, arom).  $^{13}\text{C}$  NMR (75 MHz,  $\text{CDCl}_3$ )  $\delta$  151.5, 151.4, 135.7, 135.0, 133.5, 131.3, 130.8, 130.4, 129.8, 128.6, 124.5, 122.7. Crystals, suitable for X-ray analysis, were obtained by the slow evaporation of saturated hexane/EtOAc (5/1) solution.



**18.** Red solid (71%), mp 121 °C.  $^1\text{H}$  NMR (300 MHz,  $\text{CDCl}_3$ )  $\delta$  7.57 (d,  $J = 8.7$  Hz, 1H, arom), 7.46 (d,  $J = 2.0$  Hz, 1H, arom), 7.37 (d,  $J = 8.4$  Hz, 2H, arom), 7.24 (d,  $J = 2.3$  Hz, 1H, arom), 7.12 (d,  $J = 8.4$  Hz, 2H, arom).

#### 4. Conclusions

In summary, 9 novel halogenated dichlorodiazadienes were prepared and fully characterized, while for 5 of them single crystal structures were determined. Solid state structures contained multiple Hal...Hal interactions, which were studied by DFT calculations and topological analysis of the electron density distribution within the framework of Bader's theory (QTAIM method). Calculations showed that the Hal...Hal interactions dictate a packing preference for this newly discovered class of dyes. These results further demonstrate the potential of Hal...Hal bonding in supramolecular engineering and crucial role in the stabilization of the intermolecular networks of dichlorodiazadienes. Further studies into photophysical properties of halogenated dichlorodiazadienes and their applications from our laboratory are underway and will be reported in due course.

**Supplementary Materials:** Figure S1. Visualization of electrostatic surface potentials for 10, 13–15 and 17 with selected  $V_{s,\text{min}}/V_{s,\text{max}}$  values (in kcal/mol). Table S1: Crystal data and structure refinement for 10, 13–15 and 17, Table S2. Values of the density of all electrons— $\rho(r)$ , Laplacian of electron density— $\nabla^2\rho(r)$  and appropriate  $\lambda_2$  eigenvalues (with promolecular approximation), energy density— $H_b$ , potential energy density— $V(r)$ , and Lagrangian kinetic energy— $G(r)$  (a.u.) at the bond critical points (3, -1), corresponding to Cl...F halogen-halogen contacts in 13, Table S3. Cartesian atomic coordinates for model supramolecular associates.

**Author Contributions:** Conceptualization, V.G.N. and A.G.T.; writing—review and editing; writing—original draft preparation, V.G.N., A.G.T., A.S.N.; V.G.N. and A.G.T.; software, A.S.N.; investigation, N.G.S.; A.M.M.; K.N.B.; G.T.S.; supervision, V.N.K. All authors have read and agreed to the published version of the manuscript.

**Funding:** This work was performed under the support of the FRCCP RAS State task AAAA-A19-119012990175-9. A.S.N. is grateful to Russian Science Foundation for the support of his theoretical studies (project No. 19-73-00001). We acknowledge the RUDN University Program 5-100. V.G.N. is grateful to RFBR for the support (grant N 18-03-00791).

**Conflicts of Interest:** The authors declare no conflict of interest.

#### References

- Bertani, R.; Sgarbossa, P.; Venzo, A.; Lelj, F.; Amati, M.; Resnati, G.; Pilati, T.; Metrangolo, P.; Terraneo, G. Halogen bonding in metal-organic-supramolecular networks. *Coord. Chem. Rev.* **2010**, *254*, 677–695. [CrossRef]
- Adonin, S.A.; Gorokh, I.D.; Samsonenko, D.G.; Novikov, A.S.; Korolkov, I.V.; Plyusnin, P.E.; Sokolov, M.N.; Fedin, V.P. Binuclear and polymeric bromobismuthate complexes: Crystal structures and thermal stability. *Polyhedron* **2019**, *159*, 318–322. [CrossRef]

3. Adonin, S.A.; Bondarenko, M.A.; Abramov, P.A.; Novikov, A.S.; Plyusnin, P.E.; Sokolov, M.N.; Fedin, V.P. Bromo- and Polybromoantimonates(V): Structural and Theoretical Studies of Hybrid Halogen-Rich Halometalate Frameworks. *Chem.-A Eur. J.* **2018**, *24*, 10165–10170. [[CrossRef](#)]
4. Saha, A.; Rather, S.A.; Sharada, D.; Saha, B.K. C-X...X-C vs C-H...X-C, which one is the more dominant interaction in crystal packing (X = halogen)? *Cryst. Growth Des.* **2018**, *18*, 6084–6090. [[CrossRef](#)]
5. Usoltsev, A.N.; Adonin, S.A.; Novikov, A.S.; Samsonenko, D.G.; Sokolov, M.N.; Fedin, V.P. One-dimensional polymeric polybromotellurates(IV): Structural and theoretical insights into halogen...halogen contacts. *CrystEngComm* **2017**, *19*, 5934–5939. [[CrossRef](#)]
6. Adonin, S.A.; Gorokh, I.D.; Novikov, A.S.; Abramov, P.A.; Sokolov, M.N.; Fedin, V.P. Halogen Contacts-Induced Unusual Coloring in BiIII Bromide Complex: Anion-to-Cation Charge Transfer via Br...Br Interactions. *Chem.-A Eur. J.* **2017**, *23*, 15612–15616. [[CrossRef](#)]
7. Nguyen, H.L.; Horton, P.N.; Hursthouse, M.B.; Legon, A.C.; Bruce, D.W. Halogen Bonding: A New Interaction for Liquid Crystal Formation. *J. Am. Chem. Soc.* **2004**, *126*, 16–17. [[CrossRef](#)] [[PubMed](#)]
8. Cariati, E.; Cavallo, G.; Forni, A.; Leem, G.; Metrangolo, P.; Meyer, F.; Pilati, T.; Resnati, G.; Righetto, S.; Terraneo, G.; et al. Self-complementary nonlinear optical-phores targeted to halogen bond-driven self-assembly of electro-optic materials. *Cryst. Growth Des.* **2011**, *11*, 5642–5648. [[CrossRef](#)]
9. Sun, A.; Lauher, J.W.; Goroff, N.S. Preparation of poly(diiododiacetylene), an ordered conjugated polymer of carbon and iodine. *Science* **2006**, *312*, 1030–1034. [[CrossRef](#)]
10. Metrangolo, P.; Resnati, G. Halogen Versus Hydrogen. *Science* **2008**, *321*, 918–919. [[CrossRef](#)]
11. Yang, L.; Tan, X.; Wang, Z.; Zhang, X. Supramolecular Polymers: Historical Development, Preparation, Characterization, and Functions. *Chem. Rev.* **2015**, *115*, 7196–7239. [[CrossRef](#)]
12. Maharramov, A.M.; Mahmudov, K.T.; Kopylovich, M.N.; Pombeiro, A.J.L. *Non-covalent Interactions in the Synthesis and Design of New Compounds*; John Wiley & Sons Limited: Hoboken, NJ, USA, 2016; ISBN 9781119113874.
13. Berger, G.; Frangville, P.; Meyer, F. Halogen bonding for molecular recognition: New developments in materials and biological sciences. *Chem. Commun.* **2020**, *56*, 4970–4981. [[CrossRef](#)] [[PubMed](#)]
14. Mahadevi, A.S.; Sastry, G.N. Cooperativity in Noncovalent Interactions. *Chem. Rev.* **2016**, *116*, 2775–2825. [[CrossRef](#)] [[PubMed](#)]
15. Walsh, R.B.; Padgett, C.W.; Metrangolo, P.; Resnati, G.; Hanks, T.W.; Pennington, W.T. Crystal Engineering through Halogen Bonding: Complexes of Nitrogen Heterocycles with Organic Iodides. *Cryst. Growth Des.* **2001**, *1*, 165–175. [[CrossRef](#)]
16. Teyssandier, J.; Mali, K.S.; De Feyter, S. Halogen Bonding in Two-Dimensional Crystal Engineering. *ChemistryOpen* **2020**, *9*, 225–241. [[CrossRef](#)]
17. Berger, G.; Soubhye, J.; Meyer, F. Halogen bonding in polymer science: From crystal engineering to functional supramolecular polymers and materials. *Polym. Chem.* **2015**, *6*, 3559–3580. [[CrossRef](#)]
18. Saha, B.K.; Rather, S.A.; Saha, A. Interhalogen Interactions in the Light of Geometrical Correction. *Cryst. Growth Des.* **2016**, *16*, 3059–3062. [[CrossRef](#)]
19. Bui, T.T.T.; Dahaoui, S.; Lecomte, C.; Desiraju, G.R.; Espinosa, E. The nature of halogen halogen interactions: A model derived from experimental charge-density analysis. *Angew. Chemie-Int. Ed.* **2009**, *48*, 3838–3841. [[CrossRef](#)]
20. Yang, H.; Wong, M.W. Application of halogen bonding to organocatalysis: A theoretical perspective. *Molecules* **2020**, *25*, 1045. [[CrossRef](#)]
21. Kolář, M.H.; Hobza, P. Computer Modeling of Halogen Bonds and Other  $\sigma$ -Hole Interactions. *Chem. Rev.* **2016**, *116*, 5155–5187. [[CrossRef](#)]
22. Priimagi, A.; Cavallo, G.; Forni, A.; Gorynsztein-Leben, M.; Kaivola, M.; Metrangolo, P.; Milani, R.; Shishido, A.; Pilati, T.; Resnati, G.; et al. Halogen bonding versus hydrogen bonding in driving self-assembly and performance of light-responsive supramolecular polymers. *Adv. Funct. Mater.* **2012**, *22*, 2572–2579. [[CrossRef](#)]
23. Cavallo, G.; Metrangolo, P.; Milani, R.; Pilati, T.; Priimagi, A.; Resnati, G.; Terraneo, G. The Halogen Bond. *Chem. Rev.* **2016**, *116*, 2478–2601. [[CrossRef](#)]
24. Nenajdenko, V.G.; Shastin, A.V.; Gorbachev, V.M.; Shorunov, S.V.; Muzalevskiy, V.M.; Lukianova, A.I.; Dorovatovskii, P.V.; Khrustalev, V.N. Copper-Catalyzed Transformation of Hydrazones into Halogenated Azabutadienes, Versatile Building Blocks for Organic Synthesis. *ACS Catal.* **2017**, *7*, 205–209. [[CrossRef](#)]

25. Shastin, A.V.; Sergeev, P.G.; Lukianova, A.I.; Muzalevskiy, V.M.; Khrustalev, V.N.; Dorovatovskii, P.V.; Nenajdenko, V.G. Dichloro-Substituted 1,2-Diazabuta-1,3-dienes as Highly Reactive Electrophiles in the Reaction with Amines and Diamines: Efficient Synthesis of  $\alpha$ -Hydrazo Amidinium Salts. *European J. Org. Chem.* **2018**, *2018*, 4996–5006. [[CrossRef](#)]
26. Shastin, A.V.; Tsyrenova, B.D.; Sergeev, P.G.; Roznyatovsky, V.A.; Smolyar, I.V.; Khrustalev, V.N.; Nenajdenko, V.G. Synthesis of a New Family of 1,1-Diazidoethenes: One-Pot Construction of 4-Azido-1,2,3-triazoles via Nitrene Cyclization. *Org. Lett.* **2018**, *20*, 7803–7806. [[CrossRef](#)]
27. Tsyrenova, B.; Nenajdenko, V. Synthesis and spectral study of a new family of 2,5-diaryltriazoles having restricted rotation of the 5-aryl substituent. *Molecules* **2020**, *25*, 480. [[CrossRef](#)]
28. Sergeev, P.G.; Khrustalev, V.N.; Nenajdenko, V.G. Construction of 6-Aminopyridazine Derivatives by the Reaction of Malononitrile with Dichloro-Substituted Diazadienes. *European J. Org. Chem.* **2020**, *2020*, 4964–4971. [[CrossRef](#)]
29. Shikhaliyev, N.Q.; Kuznetsov, M.L.; Maharramov, A.M.; Gurbanov, A.V.; Ahmadova, N.E.; Nenajdenko, V.G.; Mahmudov, K.T.; Pombeiro, A.J.L. Noncovalent interactions in the design of bis-azo dyes. *CrystEngComm* **2019**, *21*, 5032–5038. [[CrossRef](#)]
30. Shikhaliyev, N.Q.; Ahmadova, N.E.; Gurbanov, A.V.; Maharramov, A.M.; Mammadova, G.Z.; Nenajdenko, V.G.; Zubkov, F.I.; Mahmudov, K.T.; Pombeiro, A.J.L. Tetrel, halogen and hydrogen bonds in bis(4-(E)-(2,2-dichloro-1-(4-substitutedphenyl)vinyl)diazenyl)phenyl)methane dyes. *Dye. Pigment.* **2018**, *150*, 377–381. [[CrossRef](#)]
31. Maharramov, A.M.; Shikhaliyev, N.Q.; Suleymanova, G.T.; Gurbanov, A.V.; Babayeva, G.V.; Mammadova, G.Z.; Zubkov, F.I.; Nenajdenko, V.G.; Mahmudov, K.T.; Pombeiro, A.J.L. Pnictogen, halogen and hydrogen bonds in (E)-1-(2,2-dichloro-1-(2-nitrophenyl)vinyl)-2-(para-substituted phenyl)-diazenes. *Dye. Pigment.* **2018**, *159*, 135–141. [[CrossRef](#)]
32. Repina, O.V.; Novikov, A.S.; Khoroshilova, O.V.; Kritchenkov, A.S.; Vasin, A.A.; Tskhovrebov, A.G. Lasagna-like supramolecular polymers derived from the PdII osazone complexes via C(sp<sup>2</sup>)-H... Hal hydrogen bonding. *Inorganica Chim. Acta* **2020**, *502*, 119378. [[CrossRef](#)]
33. Tskhovrebov, A.G.; Novikov, A.S.; Odintsova, O.V.; Mikhaylov, V.N.; Sorokoumov, V.N.; Serebryanskaya, T.V.; Starova, G.L. Supramolecular polymers derived from the PtII and PdII schiff base complexes via C(sp<sup>2</sup>)-H... Hal hydrogen bonding: Combined experimental and theoretical study. *J. Organomet. Chem.* **2019**, *886*, 71–75. [[CrossRef](#)]
34. Tskhovrebov, A.G.; Vasileva, A.A.; Goddard, R.; Riedel, T.; Dyson, P.J.; Mikhaylov, V.N.; Serebryanskaya, T.V.; Sorokoumov, V.N.; Haukka, M. Palladium(II)-Stabilized Pyridine-2-Diazotates: Synthesis, Structural Characterization, and Cytotoxicity Studies. *Inorg. Chem.* **2018**, *57*, 930–934. [[CrossRef](#)]
35. Mikhaylov, V.N.; Sorokoumov, V.N.; Liakhov, D.M.; Tskhovrebov, A.G.; Balova, I.A. Polystyrene-supported acyclic diamine carbene palladium complexes in Sonogashira cross-coupling: Stability vs. catalytic activity. *Catalysts* **2018**, *8*, 141. [[CrossRef](#)]
36. Tskhovrebov, A.G.; Luzyanin, K.V.; Kuznetsov, M.L.; Sorokoumov, V.N.; Balova, I.A.; Haukka, M.; Kukushkin, V.Y. Substituent R-dependent regioselectivity switch in nucleophilic addition of N-phenylbenzamidine to PdII-and PtII-complexed isonitrile RN-C giving aminocarbene-like species. *Organometallics* **2011**, *30*, 863–874. [[CrossRef](#)]
37. Mikhaylov, V.N.; Sorokoumov, V.N.; Novikov, A.S.; Melnik, M.V.; Tskhovrebov, A.G.; Balova, I.A. Intramolecular hydrogen bonding stabilizes trans-configuration in a mixed carbene/isocyanide PdII complexes. *J. Organomet. Chem.* **2020**, *912*, 121174. [[CrossRef](#)]
38. Tskhovrebov, A.G.; Luzyanin, K.V.; Haukka, M.; Kukushkin, V.Y. Synthesis and characterization of cis-(RNC)<sub>2</sub>PtII species useful as synthons for generation of various (aminocarbene)Pt II complexes. *J. Chem. Crystallogr.* **2012**, *42*, 1170–1175. [[CrossRef](#)]
39. Tskhovrebov, A.G.; Novikov, A.S.; Kritchenkov, A.S.; Khrustalev, V.N.; Haukka, M. Attractive halogen...halogen interactions in crystal structure of trans-dibromogold(III) complex. *Zeitschrift Krist. Cryst. Mater.* **2020**. [[CrossRef](#)]
40. Bondi, A. Van der Waals volumes and radii of metals in covalent compounds. *J. Phys. Chem.* **1966**, *70*, 3006–3007. [[CrossRef](#)]
41. Bader, R.F.W. A Quantum Theory of Molecular Structure and Its Applications. *Chem. Rev.* **1991**, *91*, 893–928. [[CrossRef](#)]

42. Bartashevich, E.V.; Tsirelson, V.G. Interplay between non-covalent interactions in complexes and crystals with halogen bonds. *Russ. Chem. Rev.* **2014**, *83*, 1181–1203. [[CrossRef](#)]
43. Adonin, S.A.; Gorokh, I.D.; Novikov, A.S.; Samsonenko, D.G.; Yushina, I.V.; Sokolov, M.N.; Fedin, V.P. Halobismuthates with halopyridinium cations: Appearance or non-appearance of unusual colouring. *CrystEngComm* **2018**, *20*, 7766–7772. [[CrossRef](#)]
44. Espinosa, E.; Alkorta, I.; Elguero, J.; Molins, E. From weak to strong interactions: A comprehensive analysis of the topological and energetic properties of the electron density distribution involving X-H···F-Y systems. *J. Chem. Phys.* **2002**, *117*, 5529–5542. [[CrossRef](#)]
45. Johnson, E.R.; Keinan, S.; Mori-Sánchez, P.; Contreras-García, J.; Cohen, A.J.; Yang, W. Revealing noncovalent interactions. *J. Am. Chem. Soc.* **2010**, *132*, 6498–6506. [[CrossRef](#)] [[PubMed](#)]
46. Contreras-García, J.; Johnson, E.R.; Keinan, S.; Chaudret, R.; Piquemal, J.-P.; Beratan, D.N.; Yang, W. NCIPLOT: A Program for Plotting Noncovalent Interaction Regions. *J. Chem. Theory Comput.* **2011**, *7*, 625–632. [[CrossRef](#)] [[PubMed](#)]
47. Chai, J.-D.; Head-Gordon, M. Long-range corrected hybrid density functionals with damped atom–atom dispersion corrections. *Phys. Chem. Chem. Phys.* **2008**, *10*, 6615–6620. [[CrossRef](#)]
48. Curtiss, L.A.; McGrath, M.P.; Blaudeau, J.; Davis, N.E.; Binning, R.C.; Radom, L. Extension of Gaussian-2 theory to molecules containing third-row atoms Ga–Kr. *J. Chem. Phys.* **1995**, *103*, 6104–6113. [[CrossRef](#)]
49. Francl, M.M.; Pietro, W.J.; Hehre, W.J.; Binkley, J.S.; Gordon, M.S.; DeFrees, D.J.; Pople, J.A. Self-consistent molecular orbital methods. XXIII. A polarization-type basis set for second-row elements. *J. Chem. Phys.* **1982**, *77*, 3654–3665. [[CrossRef](#)]
50. Krishnan, R.; Binkley, J.S.; Seeger, R.; Pople, J.A. Self-consistent molecular orbital methods. XX. A basis set for correlated wave functions. *J. Chem. Phys.* **1980**, *72*, 650–654. [[CrossRef](#)]
51. McLean, A.D.; Chandler, G.S. Contracted Gaussian basis sets for molecular calculations. I. Second row atoms, Z=11–18. *J. Chem. Phys.* **1980**, *72*, 5639–5648. [[CrossRef](#)]
52. Lu, T.; Chen, F. Multiwfn: A multifunctional wavefunction analyzer. *J. Comput. Chem.* **2012**, *33*, 580–592. [[CrossRef](#)]
53. Spackman, M.A.; Jayatilaka, D. Hirshfeld surface analysis. *CrystEngComm* **2009**, *11*, 19–32. [[CrossRef](#)]
54. McKinnon, J.J.; Jayatilaka, D.; Spackman, M.A. Towards quantitative analysis of intermolecular interactions with Hirshfeld surfaces. *Chem. Commun.* **2007**, 3814–3816. [[CrossRef](#)] [[PubMed](#)]
55. Evans, P. Scaling and assessment of data quality. *Acta Crystallogr. Sect. D Biol. Crystallogr.* **2006**, *62*, 72–82. [[CrossRef](#)]
56. Battye, T.G.G.; Kontogiannis, L.; Johnson, O.; Powell, H.R.; Leslie, A.G.W. iMOSFLM: A new graphical interface for diffraction-image processing with MOSFLM. *Acta Crystallogr. Sect. D Biol. Crystallogr.* **2011**, *67*, 271–281. [[CrossRef](#)] [[PubMed](#)]
57. Winn, M.D.; Ballard, C.C.; Cowtan, K.D.; Dodson, E.J.; Emsley, P.; Evans, P.R.; Keegan, R.M.; Krissinel, E.B.; Leslie, A.G.W.; McCoy, A.; et al. Overview of the CCP4 suite and current developments. *Acta Crystallogr. Sect. D Biol. Crystallogr.* **2011**, *67*, 235–242. [[CrossRef](#)]
58. Sheldrick, G.M. SHELXT—Integrated space-group and crystal-structure determination. *Acta Crystallogr. Sect. A Found. Crystallogr.* **2015**, *71*, 3–8. [[CrossRef](#)]
59. Sheldrick, G.M. A short history of SHELX. *Acta Crystallogr. A* **2008**, *64*, 112–122. [[CrossRef](#)]
60. Sheldrick, G.M. Crystal structure refinement with SHELXL. *Acta Crystallogr. Sect. C Struct. Chem.* **2015**, *71*, 3–8. [[CrossRef](#)]

**Sample Availability:** Samples of the compounds 1–18 are available from the authors.

**Publisher’s Note:** MDPI stays neutral with regard to jurisdictional claims in published maps and institutional affiliations.



© 2020 by the authors. Licensee MDPI, Basel, Switzerland. This article is an open access article distributed under the terms and conditions of the Creative Commons Attribution (CC BY) license (<http://creativecommons.org/licenses/by/4.0/>).